# Superresolution microscopy reveals structural mechanisms driving the nanoarchitecture of a viral chromatin tether

Margaret J. Grant[a], Matthew S. Loftus[a], Aiola P. Stoja[a], Dean H. Kedes[a,b,1], and M. Mitchell Smith[a,1]

[a]Department of Microbiology, Immunology and Cancer Biology, University of Virginia, Charlottesville, VA 22908; and [b]Department of Medicine, Division of Infectious Diseases and International Health, University of Virginia, Charlottesville, VA 22908

Edited by Donald E. Ganem, Novartis Institutes for Biomedical Research, Inc., Emeryville, CA, and approved March 2, 2018 (received for review December 13, 2017)

**By tethering their circular genomes (episomes) to host chromatin, DNA tumor viruses ensure retention and segregation of their genetic material during cell divisions. Despite functional genetic and crystallographic studies, there is little information addressing the 3D structure of these tethers in cells, issues critical for understanding persistent infection by these viruses. Here, we have applied direct stochastic optical reconstruction microscopy (dSTORM) to establish the nanoarchitecture of tethers within cells latently infected with the oncogenic human pathogen, Kaposi's sarcoma-associated herpesvirus (KSHV). Each KSHV tether comprises a series of homodimers of the latency-associated nuclear antigen (LANA) that bind with their C termini to the tandem array of episomal terminal repeats (TRs) and with their N termini to host chromatin. Superresolution imaging revealed that individual KSHV tethers possess similar overall dimensions and, in aggregate, fold to occupy the volume of a prolate ellipsoid. Using plasmids with increasing numbers of TRs, we found that tethers display polymer power law scaling behavior with a scaling exponent characteristic of active chromatin. For plasmids containing a two-TR tether, we determined the size, separation, and relative orientation of two distinct clusters of bound LANA, each corresponding to a single TR. From these data, we have generated a 3D model of the episomal half of the tether that integrates and extends previously established findings from epifluorescent, crystallographic, and epigenetic approaches. Our findings also validate the use of dSTORM in establishing novel structural insights into the physical basis of molecular connections linking host and pathogen genomes.**

KSHV | LANA | terminal repeat | dSTORM | DNA bending

Kaposi's sarcoma-associated herpesvirus (KSHV) is the etiological agent of Kaposi's sarcoma, an inflammatory tumor of the skin and mucous membranes, as well as two B-cell tumors, primary effusion lymphoma (PEL) and multicentric Castleman's disease (1–3). KSHV infection is marked by long periods of latency when the virus expresses only a small number of essential genes (4). Among these is ORF73 that encodes LANA (5, 6), a protein of 1,162 amino acids with multiple functions, including the tethering of viral episomes to host chromatin. The N termini of LANA dimers bind to histones H2A/B and to chromatin-associated bromodomain proteins (7–10). The C termini of three LANA dimers bind to three adjacent 20-bp LANA binding sites (LBSs 1, 2, and 3) located in each 801-bp terminal repeat (TR) (Fig. 1*A*) (11–15). There are an estimated 35 to 60 tandem TRs per viral episome (16, 17), arranged head to tail at a single location on the circular episome. The resulting tether, comprising this cluster of TRs and bound LANA dimers, is essential for episomal maintenance within dividing cells and, presumably, persistence in patients (12, 18–21). Initial epifluorescence studies identified LANA as nuclear punctae recognized by serum antibodies from KSHV-infected patients (22–25). Ten years later, Adang et al. (26) used a combination of flow cytometry and qPCR to demonstrate a direct proportionality between the number of LANA punctae and the amount of viral DNA, leading to the conclusion that each nuclear dot represented a single viral episome. Previous studies examining these punctae showed association of LANA with mitotic chromosomes at the resolution of epifluorescence microscopy (12, 27). Kelley-Clarke et al. (28) later suggested preferential localization of these LANA punctae to centromeric and telomeric regions on metaphase chromosome. Such studies have provided a solid foundation for further inquiry into the nature of this tethering mechanism.

Many fundamental features of full-length tethers in cells have remained elusive due to the resolution constraints of epifluorescence microscopy. While X-ray crystallography has resolved the structures of an N-terminal 23 amino acid LANA peptide bound to nucleosomes, and a C-terminal 139 amino acid peptide in complex with LBS1 (7, 15), questions remain as to the architectural features of a full-length tether. It is unknown how TR chromatin folds and whether this is consistent among tethers, both within and across cell lines. The close packing of nucleosomes

## Significance

**Kaposi's sarcoma-associated herpesvirus propagates by attaching to host chromatin. This tether is essential for viral maintenance, and its disruption represents a potential treatment for persistent infection. However, fundamental questions remain, including how the underlying viral chromatin is folded, how the tether protein is organized, and how it is presented for host attachment. Using superresolution fluorescence microscopy, we have visualized single tethers in cells and built a working model of their structure. The folding of the viral chromatin mimics that of active chromatin, driven by nucleosome positioning and DNA bending. Furthermore, tether proteins are arranged in ordered clusters projected outward from the viral chromatin axis. These principles are likely to be applicable to the tethers of other DNA tumor viruses.**

Author contributions: M.J.G., D.H.K., and M.M.S. designed research; M.J.G., M.S.L., A.P.S., and M.M.S. performed research; M.J.G. and M.M.S. contributed new reagents/analytic tools; M.J.G., M.S.L., A.P.S., D.H.K., and M.M.S. analyzed data; M.J.G., D.H.K., and M.M.S. wrote the paper; M.J.G. and D.H.K. codesigned experiments; D.H.K. and M.M.S. contributed to the conception of the project; M.M.S. conducted and analyzed the dSTORM microscopy; and M.S.L. and A.P.S. contributed to determining the BCBL-1 TR copy number and the two-TR nucleotide sequence, respectively.

The authors declare no conflict of interest.

This article is a PNAS Direct Submission.



Data deposition: The DNA sequence of the TR region of p2TR reported in this paper has been deposited in the GenBank database (accession no. MG963161).

See Commentary on page 4816.

[1]To whom correspondence may be addressed. Email: mms7r@Virginia.EDU or kedes@virginia.edu.

This article contains supporting information online at www.pnas.org/lookup/suppl/doi:10.1073/pnas.1721638115/-/DCSupplemental.

Published online April 2, 2018.

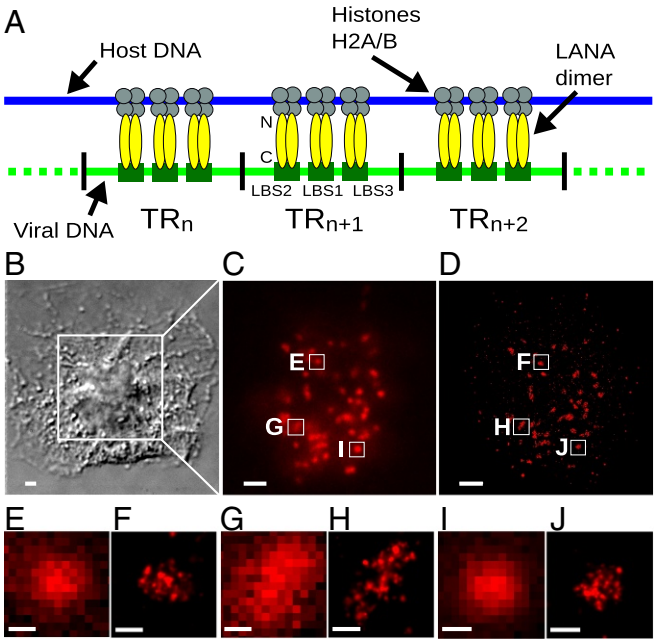


**Fig. 1.** dSTORM offers improved image resolution of LANA tethers. (*A*) Schematic depiction of the anatomy of a KSHV LANA tether. LANA dimers (shown in yellow) bind via their N termini to histones H2A/B (gray). The C termini bind with sequence specificity to three LBSs located on each TR. (*B*) An anti-LANA stained BCBL-1 cell imaged by differential interference contrast microscopy. (*C*) The boxed region in *B* viewed by conventional epifluorescence microscopy. (*D*) The same field of view as in *C* imaged by dSTORM microscopy. (Scale bars for *B–D*, 2 μm.) (*E*, *G*, and *I*) The three LANA tethers boxed in *C* are enlarged for better visualization. (*F*, *H*, and *J*) The three LANA tethers boxed in *D* are enlarged for comparison with their paired standard epifluorescence images (*E*, *G*, and *I*). (Scale bars for *E–J*, 250 nm.)

and presence of heterochromatin protein 1 (HP1) at TRs supports heterochromatin conformation, whereas epigenetic, replication, and transcription studies suggest active chromatin (14, 29–33). Questions also remain as to how LANA is distributed across the TRs, whether it attains full occupancy on all three LBSs, and whether supernumerary LANA dimers form large complexes at each TR to entrap episomal DNA loops (34). There is also no information indicating whether the number of TRs bound by LANA reaches a plateau. LANA dimers might bind to a maximum number of TRs in a plasmid or episome, regardless of the number of total TRs available. Finally, it is not clear how all of these elements influence tether folding and the ability to effectively bind to both viral and host genomes. To address these questions, we applied superresolution microscopy to study KSHV-infected cells with the goal of generating architectural data on full-length KSHV tethers.

## Results

**The Nanoscale Dimensions of LANA Tethers Are Uniform and Consistent Across Different Cell Types.** In principle, since LANA binds both host nucleosomes and episome DNA, the packaging of TR chromatin could be determined primarily by the state of the host chromatin, by features intrinsic to the viral episome, or both. To distinguish among these alternatives, we examined the tether morphology of the same viral isolate in two different cell types. We found that direct stochastic optical reconstruction microscopy (dSTORM) resolved each epifluorescent LANA dot into a cluster of individual emissions from fluorophore-labeled anti-LANA mAbs (Fig. 1 *B–J*). We interpret these emissions as blinks within a Gaussian localization volume from each conjugated dye molecule present at approximately three dye molecules per mAb (*Supporting Information*), up to six mAbs bound per LANA dimer (see *The 2TR Images Support the Prediction of a LANA Coiled-Coil Domain*), and up to three LANA dimers per TR. Since all of the episomes from the same virus have the same number of TRs (17, 35), and each TR is 801 bp, we asked whether the polymer architectures revealed by dSTORM would be similarly consistent across multiple tethers. We examined 65 individual LANA tethers from BCBL-1 cells (a KSHV-positive PEL line) and 34 from SLKp/Caki-1p cells, a human epithelial line exogenously infected with KSHV derived from BCBL-1 (36, 37). We found that, while each tether presented a unique shape, their overall dimensions were similar in the two cell lines (Fig. 2 *A* and *B*). To quantify this similarity, we aligned clusters along their three principal axes and calculated their dimensions and radii of gyration, $R_g$ (see *Supporting Information*), shown in Fig. 2 *C* and *D*. The median $R_g$ for tethers in BCBL1 cells was 341 nm, 95% CI [309, 353] and in SLKp cells it was 368 nm, 95% CI [323, 405]. There was no statistical difference between the $R_g$ of BCBL-1 and SLKp tethers ($P = 0.26$, Mood's Median Test). The similarity of these parameters in a single viral strain in two different cell types shows that the polymer folding of KSHV LANA tethers is likely to be intrinsic to the viral episome itself, rather than being a result of the cellular milieu.

**LANA Occupancy Scales with the Number of TRs.** We postulated that, if the tethers visualized by dSTORM reflect the underlying

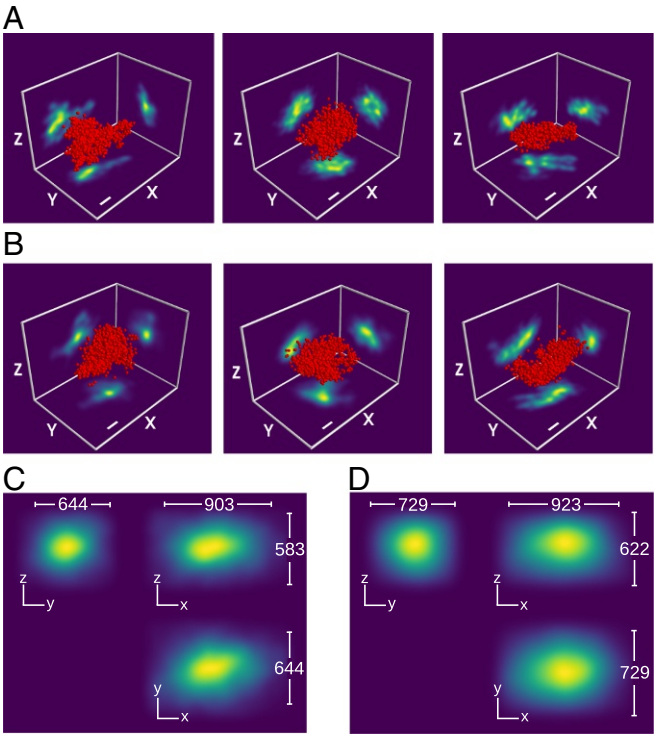


**Fig. 2.** KSHV LANA tethers have consistent dimensions within and between cell types. (*A*) The 3D projections of three representative LANA tethers from asynchronous BCBL-1 cells. Red spheres depict the Cartesian coordinates of individual photon emissions, with their radii scaled to the median axial localization precision of 30 nm. (*B*) Three representative LANA tethers from asynchronous SLKp cells, shown as in *A*. (Scale bars for *A* and *B*, 250 nm.) (*C*) LANA tethers from BCBL-1 cells ($n = 65$) were oriented by principal axes and aligned at their centroids. The compilation is rendered as Gaussian emissions with 30-nm localization precision and presented from three architectural viewpoints, indicated by the *x*, *y*, and *z* directional axes. Median dimensions are shown by the bars. (*D*) LANA tethers from SLKp cells ($n = 34$) superimposed and rendered as in *C*.

TR architecture, then their structural parameters should change systematically with different numbers of TR elements. To challenge that hypothesis, we examined synthetic tethers with different numbers of TRs. We cotransfected BJAB cells, a KSHV-negative human B-cell line, with two plasmids, one encoding LANA and the other containing two, five, seven, or eight tandem TRs arranged head to tail as in the native episome (Fig. S1 *A* and *B*). In addition, we infected BJAB cells with BAC16 virus that we determined contains approximately 21 TRs (Fig. S1 *C* and *D*). Transfection with a LANA-encoding plasmid and a plasmid lacking any functional TR sequence (p0TR) resulted only in diffuse nuclear staining by epifluorescence (Fig. S2*A*), consistent with earlier work (12, 38). In contrast, individual tethers in cells harboring plasmids with 2, 8, or 21 TRs showed a progressive increase in size (Fig. 3 *A*–*C*). Accompanying this increase was a corresponding linear rise in the number of dSTORM fluorophore emissions and, therefore, anti-LANA Ab binding (Fig. 3*D*). Our observation that an increase in TR number results in a proportional increase in LANA binding argues against a plateau for TR occupancy per plasmid or episome, at least over the range of 1 to 21 TRs.

**Tether Polymer Conformation Has the Characteristics of Active Chromatin.** At present, there is conflicting evidence regarding the conformation of TR chromatin, which exhibits features of both repressed and active conformations. On one hand, TR nucleosomes are tightly packed in a typically "closed" conformation (31). Furthermore, LANA recruits the histone H3 methyltransferase SUV39H1 and establishes HP1 binding to the TR chromatin (30). In contrast, in support of an active conformation, TR chromatin is marked by histone hyperacetylation (29, 31, 32) associated with bromodomain protein BRD4 (9, 39), and the TRs have both promoter and origin of replication functions (14, 33).

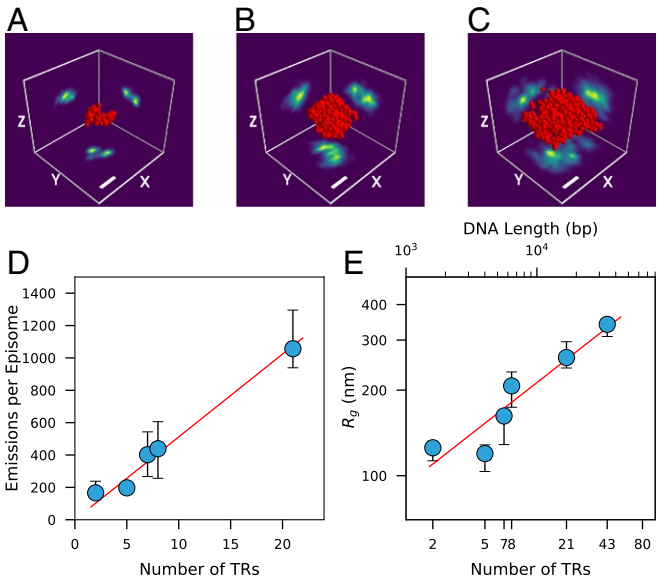


**Fig. 3.** LANA tethers show polymer-like scaling as a function of the number of TRs. (*A*–*C*) The 3D projections of representative LANA tethers from a cell transfected with (*A*) p2TR, (*B*) p8TR, or (*C*) BAC16 with 21 TRs are shown at identical scales as described in Fig. 2. (Scale bar for *A*–*C*, 250 nm.) (*D*) The linear relationship between the median number of emissions and the number of TRs per tether is shown for p2TR ($n$ = 28), p5TR ($n$ = 39), p7TR ($n$ = 13), p8TR ($n$ = 17), and BAC16 ($n$ = 32) ($R^2 = 0.99$). (*E*) The log of median $R_g$ data for the tethers in *D* and BCBL-1 KSHV episomes (43 TRs, $n$ = 65) are shown as a function of the log of the tether DNA lengths (top axis) or the log of the TR number (bottom axis). The regression (solid red line) through tethers with known numbers of TRs (blue circles) was used to calculate the scaling exponent $c = 0.36 \pm 0.07$ ($R^2 = 0.94$). Error bars represent 95% CIs.

To address the conformational state directly, we took advantage of the fact that the radius of gyration, $R_g$, of a chromatin polymer follows the power law relationship, $R_g \propto L^c$, where $L$ is the DNA length in base pairs and $c$ is the scaling exponent. This scaling parameter is a sensitive measure of canonical active, inactive, and repressed states of mammalian chromatin (40). By plotting $R_g$ against $L$, we determined the power law scaling exponent for the LANA-bound TR chromatin to be $c = 0.36 \pm 0.07$ (Fig. 3*E*). This exponent approximated the value of $0.37 \pm 0.02$ found by Boettiger et al. (40) for active chromatin and is distinct from values for inactive ($c = 0.30 \pm 0.02$) or repressed ($c = 0.22 \pm 0.02$) chromatin. We obtained similar results for TR plasmid scaling in COS-7 cells (Fig. S3*A*). This finding clarifies the long-standing paradox surrounding the chromatin folding state of the TR region.

**Adjacent TRs Are Arranged with a Specific Asymmetric Architecture.** Closer analysis of the dSTORM emissions from individual p2TR tethers revealed that they frequently gave rise to two distinct, resolvable clusters (Fig. 3*A*), and alignment of the complete set of 28 p2TR data (see *Supporting Information*) reinforced this separation (Fig. 4*A*). Individual clusters had an $R_g$ of 90 nm, 95% CI [82, 96], which is similar to the $R_g$ of 86 nm predicted by extrapolation of the power law function to a single TR (Fig. 3*E*). Thus, we interpreted the two clusters as the signals emanating from two adjacent TRs. We obtained similar results for p2TR dSTORM images acquired in COS-7 cells (Fig. S3*B*). The p2TR tethers, individually or as an aligned composite, showed striking asymmetry. They comprised flat pairs of prominently elongated ellipsoids whose centroids were spaced apart by 174 nm, 95% CI [152, 185] (Fig. 4*B*). Moreover, the long axes of the two clusters intersected to form a 46° angle (Fig. 4*B*), demonstrating a specific differential placement of the individual TRs within the p2TR structure. These parameters provided strong constraints on the underlying folding of the p2TR chromatin tether.

**The 2TR Images Support the Prediction of a LANA Coiled-Coil Domain.** To begin to interpret the 2TR tether images at the molecular level, we evaluated the structure of LANA dimers N-terminal to the LBS binding domains, for which previous X-ray crystal structures are known (10, 15, 39). Examination of the primary protein sequence of LANA with Paircoil2 (41) revealed a segment strongly predicted to form a coiled coil (Fig. S4*A*; $P < 0.025$). To test for the presence of the coiled coil, we measured the number of single-molecule emissions detected by dSTORM for LANA tethers stained with LN53-A647, which recognizes the tetrapeptide epitope EQEQ (42). There are 22 such epitopes within the LANA protein sequence, and this number of mAbs would yield over 18,000 dSTORM emissions per tether (see *Supporting Information*). However, 19 of the most C-terminal of these epitopes would be embedded within the putative coiled-coil region of LANA, occluding mAb recognition. The remaining three epitopes just N-terminal to the coiled coil would yield on the order of only 2,500 emissions per tether. Indeed, we routinely recovered fewer than 2,000 emissions per tether, consistent with only two to three functional epitopes per LANA protein, providing strong empiric data for the predicted coiled coil. Furthermore, the positioning of these available epitopes at the N-terminal end of a rigid coiled-coil domain is supported by the separation between the two emissions clusters in the 2TR images. We generated a molecular model of LANA dimers incorporating these features (Fig. S4).

**LANA-Imposed DNA Bending and Nucleosome Translational Positioning Are Predicted to Direct TR Chromatin Folding.** Although the DNA of each TR is known to be bent by LANA dimer binding (15, 43, 44), and to be occupied by four nucleosomes (31),

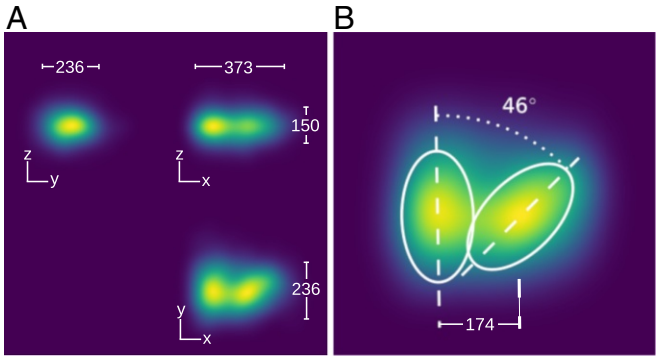


**Fig. 4.** p2TR tethers show two distinct clusters of LANA Ab that form a 46° angle between their long axes. (*A*) Compilation of emission data from 28 p2TR tethers; emissions are rendered as in Fig. 2. Median dimensions (nanometers) of the combined data are shown. (*B*) Approximately 2× magnified view of the *y*–*x* projection from *A* demonstrating the 46° angle formed between the two clusters.

the constraints these factors impose on tether architecture are currently unknown. To address this question, we varied the parameters of DNA bending and nucleosome positioning in a set of molecular models (Fig. S5). We modeled the 113 bp of nucleosome-free DNA that contains the three LBS sites in two modes. In the first, both LBS1 and LBS2 are occupied by LANA dimers, while LBS3 is unoccupied, inducing a 110° bend in LBS DNA (Fig. S5*C*), as previously determined by Wong and Wilson (43). In the second mode, LBS1, LBS2, and LBS3 are all occupied by LANA dimers, inducing a bend of ∼180° (Fig. S5*D*), as predicted by Hellert et al. (15). For the remaining 688 bp of TR DNA occupied by four nucleosomes, we adapted the crystal structure of a synthetic tetrasome [Protein Data Bank (PDB) ID 1ZBB] (45) because of its similarity to the spacing of the nucleosomes mapped to the TR (31) (Fig. S5*B*). We digitally joined the tetrasome DNA to the LBS DNA, bent at either 110° (Fig. S5*E*) or 180° (Fig. S5*F*). We varied the position of the joint by a single base pair at a time over a 9-bp span, designated phases 1 to 9, to model the effect of nucleosome translational positioning on tether architecture through an entire turn of a DNA helix (Fig. S6 *A* and *E*). Each base pair change in the nucleosome phasing changes the trajectory of the chromatin fiber by approximately 36° (1/10 of a full turn). To extend the model to include two adjacent TRs, we joined pairs of these single TR models at each of the nine nucleosome phases to produce the complete set of 81 2TR models (nine phases for each tetrasome) (Fig. S6 *B* and *F*), keeping the repeat length at 801 bp between LBS1 sites. For models with occupancy of only LBS1 and LBS2, we eliminated 11 of the 81 combinations from further consideration based on steric interference, either between two tetrasomes or the trajectory of connecting DNA (shown in purple and blue, Fig. S6*B*). For the models with full occupancy of three LBS sites, 50 models were ruled out (shown in purple and blue, Fig. S6*F*). Examples of 2TR phase combinations with or without steric hindrance are depicted in Fig. S6. The impact of both LANA-dependent DNA bending and nucleosome translational positioning on the construction of these 2TR models, and the ability of these parameters to eliminate certain tetrasome configurations, demonstrates the importance of these two factors for tether architecture.

**A Simple Molecular Model Captures Major Properties of 2TR LANA Tethers.** Remarkably, our 2TR models captured key features of the dSTORM images. In particular, the model with full LANA occupancy of all three LBSs on both TRs and the second tetrasome joined to the DNA at "phase 8" mimicked features of the image (Fig. 5*A*, and see also Fig. S6*E*). The addition of three LANA dimers to each TR of the 2TR model produced an elongated arrangement of epitope binding sites and predicted the localization of their associated dye emissions. Furthermore, the long axes joining the epitope binding sites on each TR give rise to approximately a 45° angle between them by the combination of tetranucleosome positioning and LBS DNA bending. The distance between the centers of the two sets of epitopes was ∼151 nm. Both the angle and spacing of emissions in the model approximated those of the experimental data (Fig. 4*B*).

We tested the ability of our chromatin models to account for the dSTORM data of individual tethers by optimizing the fit of the modeled epitope sites (dye locations) to the experimental p2TR emissions data (see *Supporting Information*). We then determined the best-fit models by scoring each by the fraction of dSTORM emissions that they captured. One example of such a fit is shown in Fig. 5*B* and Movie S1.

In a pair-wise comparison of models with LANA dimers at all three LBS sites versus models with LANA dimers only at LBS1 and LBS2, the full occupancy models were significantly better at accounting for the 28 p2TR datasets ($P < 3.0 \times 10^{-12}$, Paired *t* test). Overall, the median fraction of dSTORM emissions accounted for by the optimal full occupancy models was 0.72, 95% CI [0.61, 0.83] (Fig. 5*C*) for the p2TR structures assembled in BJAB cells. We carried out the same analysis of p2TR LANA tethers expressed in COS-7 cells and found the median fraction of emissions covered to be 0.78, 95% CI [0.66, 0.94] (Fig. S3 *C* and *D*). Interestingly, the optimal phasing between TRs was not the same for all 2TR tethers examined. Rather, this parameter varied from tether to tether, with phases 5 to 9 each contributing to the set of best-fit models (Fig. S7). This range of phases suggests a basis for the shape variability seen among the individual LANA tethers comprised of larger numbers of TRs (Fig. 2).

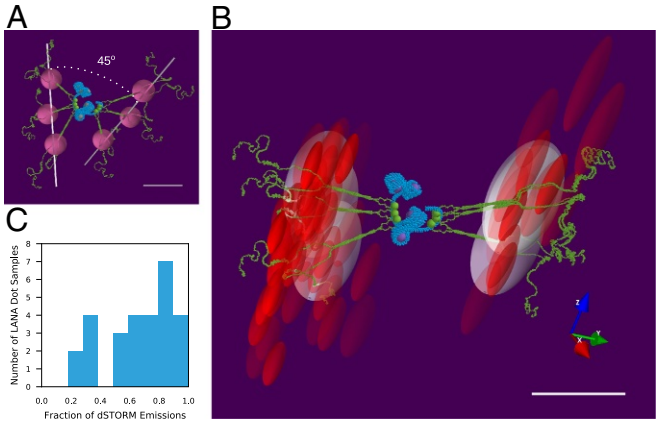


**Fig. 5.** dSTORM analysis of p2TR tethers is consistent with a model featuring full LBS and nucleosome occupancy on two sequential TRs. (*A*) Model depicting two TRs (blue), each containing four nucleosomes (gray) and bound by three LANA dimers (green) occupying LBSs. Predicted coiled-coil portions of LANA dimers extend outward at approximately right angles to the LBSs. Magenta spheres depict the position of a 13-nm-long anti-LANA mAb. Two white lines represent the best linear fit connecting three LANA dimers for each TR, forming a 45° angle. (*B*) Data from one p2TR example aligned with the model in *A*. Red ellipsoids depict the probability volume of individual fluorophore emissions, scaled by their lateral and axial localization precision. White ellipsoids depict the model-predicted probability volumes scaled by data-derived localization precision. (*C*) Histogram displaying the distribution of the fraction of observed emissions whose localization precision volumes intersect with the model-predicted volume. (Scale bars, 50 nm.)

## Discussion

Until now, LANA tethers have appeared as poorly defined nuclear punctae via epifluorescence microscopy. The localization data from this study offer insights into the architecture of the tethers linking KSHV episomes to human chromatin. First, we found that the folding of tether chromatin was intrinsic to the viral episome and independent of the cellular environment. Consistent shapes and emission counts were measured for comparable TR episomes within the B-cell–derived lines BCBL-1 and BJAB, the nonlymphocytic epithelial cell line SLKp, and even the monkey kidney fibroblast cell line COS-7. Second, regardless of the number, TRs were proportionally occupied by LANA dimers. This argues for a relatively uniform chromatin environment across the terminal repeats wherein LBS sites are equally accessible to LANA binding in all TRs. Third, we provided physical proof that TR chromatin folds with parameters characteristic of active chromatin, likely driven by nucleosome-free regions in the TRs, helping to clarify conflicting evidence pertaining to the chromatin state (14, 29–33). Fourth, the ability of dSTORM to resolve single TR units within 2TR clusters demonstrates that the episomal half of LANA dimers must be well ordered. If LANA dimers radiated randomly from the LBSs or were highly unstructured in their episomal half, we would be unable to separate discrete clusters in the analyses of plasmids containing two TRs. Finally, our data argue that all three LBS sites in individual TRs are likely to be fully occupied by LANA dimers. The discrete dimensions and positional asymmetry of the dye emission clusters in the 2TR data are not well accounted for if only two LBS sites are occupied, because the axis through the epitopes of each TR is shortened and there is less bending of the LBS DNA. Furthermore, models with three LANA dimers per TR consistently performed better than models with only two LANA dimers per TR in explaining dSTORM data for 26 independent 2TR datasets. The linear relationship between LANA dye emissions and TR number suggests that this is true for complete KSHV episomes as well.

We identified several key features of tether structure by modeling the 2TR data. First, the modeling revealed that the internal repeats of LANA likely comprise a coiled-coil domain for the LANA dimer. This domain was first predicted by in silico analysis, and then supported by quantitative analysis of LN53 mAb binding, and masks all but the two to three N-terminal most mAb binding sites. Second, the modeling highlighted an impact of translational positioning of the nucleosomes for each TR. Moving each tetranucleosome along the nine possible phases of the DNA helix alters the trajectory of the output TR DNA. This, in turn, greatly impacts the relative positions of the LBSs on adjacent TRs and, hence, their associated anti-LANA fluorophore emissions. The architecture driven by nucleosome positioning and LBS DNA bending positions the LANA N-terminal histone binding domains in a way that facilitates exploration of the surrounding environment, promoting their primary function of tethering to host chromatin.

While the 2TR model describes most of the tethers well, a few datasets are exceptions mainly due to their having relatively larger $R_g$ values. Others have proposed large multi-LANA dimer complexes based on crystallography of the C-terminal binding domain (10, 15, 39), and it is possible these 2TR exceptions reflect such assemblies. Further, our current model has some limitations. For example, it is unlikely that the fixed packing of tetranucleosomes we adapted from the crystallographic structure reflects the full range of conformations adapted by TR nucleosomes in vivo. Unlike the KSHV tether histones, the histones present in the tetranucleosome crystal structure lacked any posttranslational modifications. The presence of such modifications might alter the tetrasome structure, potentially loosening or tightening the histone packing, and thereby impact our model and its fit to our data.

Recently, Chiu et al. (46) described the clustering of a subset of KSHV episomes. In our study, we focused on individual TR structures at single-molecule localization precision (10 nm to 30 nm) and excluded any ambiguous structures from our analyses. We occasionally noted single bright LANA dots by epifluorescence, but, most often, dSTORM resolved these into distinct LANA tethers. In these cases, the N termini of the LANA tethers might have also clustered episomes as Chiu et al. suggest.

Our current working model captures major features of the KSHV tether, detailing the likely stoichiometry and relative positions of its major molecular components emanating from the TR region of the viral genome within the cellular milieu. The model also provides a platform for future experimentation that could include determining the nanoarchitecture of tethers with greater numbers of TRs. This approach has broad applicability to a wide variety of persistent viral pathogens, thus potentially contributing to our ability to target them therapeutically.

## Materials and Methods

**Cell Lines.** BCBL-1 cells have been in the laboratory of D.H.K., who was a coauthor on the study first describing the line (47). BJAB cells (48) were a gift from Don Ganem, Novartis Institutes for Biomedical Research, Emeryville, CA. SLKp/Caki-1p cells (37) were a gift from Adam Grundhoff, Heinrich Pette Institute, Leibniz Institute for Experimental Virology, Hamburg, Germany, and Don Ganem (36). iSLK-BAC16 cells (49) were a gift from Rolf Renne, University of Florida, Gainesville, FL. COS-7 cells were a gift from Jim Casanova, University of Virginia, Charlottesville, VA.

**Plasmids.** The pcDNA3-LANA plasmid (50) was a gift from Rolf Renne, University of Florida. The p8TR plasmid (12) was produced by the laboratory of Kenneth Kaye, Harvard Medical School, Boston, and was a gift from Paul Lieberman, The Wistar Institute, Philadephia. The construction of plasmids containing zero, two, five, and seven terminal repeats is described in *SI Materials and Methods*.

**Antibodies.** The anti-LANA antibody LN53 (rat, monoclonal) (51) was conjugated using an Alexa Fluor 647 succinimidyl ester kit (Thermo Fisher Scientific).

**dSTORM Microscopy.** The instrumentation, sample preparation, image acquisition, and data analysis for dSTORM imaging are described in *SI Materials and Methods*.

**ACKNOWLEDGMENTS.** We thank Barbara Knowles, Samuel Hess, Travis Gould, and Mudalige Gunewardene for an introduction to superresolution microscopy and advice on instrumentation, and Stefan Bekiranov for discussions. This work was supported, in part, by the University of Virginia Cancer Center Grant P30CA044579 (to D.H.K. and M.M.S.). D.H.K. acknowledges support of the National Institute of Dental and Craniofacial Research Award R01DE022291. M.M.S. acknowledges support of the National Institute of General Medical Sciences Awards RC1GM091175 and R01GM116994.

1. Chang Y, et al. (1994) Identification of herpesvirus-like DNA sequences in AIDS-associated Kaposi's sarcoma. *Science* 266:1865–1869.
2. Cesarman E, Chang Y, Moore PS, Said JW, Knowles DM (1995) Kaposi's sarcoma–associated herpesvirus-like DNA sequences in AIDS-related body-cavity–based lymphomas. *New Engl J Med* 332:1186–1191.
3. Soulier J, et al. (1995) Kaposi's sarcoma-associated herpesvirus-like DNA sequences in multicentric Castleman's disease [see comments]. *Blood* 86:1276–1280.
4. Dittmer D, et al. (1998) A cluster of latently expressed genes in Kaposi's sarcoma-associated herpesvirus. *J Virol* 72:8309–8315.
5. Kedes DH, Lagunoff M, Renne R, Ganem D (1997) Identification of the gene encoding the major latency-associated nuclear antigen of the Kaposi's sarcoma-associated herpesvirus. *J Clin Invest* 100:2606.
6. Rainbow L, et al. (1997) The 222- to 234-kilodalton latent nuclear protein (LNA) of Kaposi's sarcoma-associated herpesvirus (human herpesvirus 8) is encoded by orf73 and is a component of the latency-associated nuclear antigen. *J Virol* 71:5915–5921.
7. Barbera AJ (2006) The nucleosomal surface as a docking station for Kaposi's sarcoma herpesvirus LANA. *Science* 311:856–861.

8. Barbera AJ, Chodaparambil JV, Kelley-Clarke B, Luger K, Kaye KM (2006) Kaposi's sarcoma-associated herpesvirus LANA hitches a ride on the chromosome. *Cell Cycle* 5:1048–1052.
9. You J, et al. (2006) Kaposi's sarcoma-associated herpesvirus latency-associated nuclear antigen interacts with bromodomain protein Brd4 on host mitotic chromosomes. *J Virol* 80:8909–8919.
10. Hellert J, et al. (2013) A structural basis for BRD2/4-mediated host chromatin interaction and oligomer assembly of Kaposi sarcoma-associated herpesvirus and murine gammaherpesvirus LANA proteins. *PLoS Pathog* 9:e1003640.
11. Russo JJ, et al. (1996) Nucleotide sequence of the Kaposi sarcoma-associated herpesvirus (HHV8). *Proc Natl Acad Sci USA* 93:14862–14867.
12. Ballestas ME (1999) Efficient persistence of extrachromosomal KSHV DNA mediated by latency-associated nuclear antigen. *Science* 284:641–644.
13. Garber AC, Shu MA, Hu J, Renne R (2001) DNA binding and modulation of gene expression by the latency-associated nuclear antigen of Kaposi's sarcoma-associated herpesvirus. *J Virol* 75:7882–7892.
14. Garber AC, Hu J, Renne R (2002) Latency-associated nuclear antigen (LANA) cooperatively binds to two sites within the terminal repeat, and both sites contribute to the ability of LANA to suppress transcription and to facilitate DNA replication. *J Biol Chem* 277:27401–27411.
15. Hellert J, et al. (2015) The 3D structure of Kaposi sarcoma herpesvirus LANA C-terminal domain bound to DNA. *Proc Natl Acad Sci USA* 112:6694–6699.
16. Lagunoff M, Ganem D (1997) The structure and coding organization of the genomic termini of Kaposi's sarcoma-associated herpesvirus (human herpesvirus 8). *Virology* 236:147–154.
17. Judde JG, et al. (2000) Monoclonality or oligoclonality of human herpesvirus 8 terminal repeat sequences in Kaposi's sarcoma and other diseases. *J Natl Cancer Inst* 92:729–736.
18. Ballestas ME, Kaye KM (2001) Kaposi's sarcoma-associated herpesvirus latency-associated nuclear antigen 1 Mediates episome persistence through cis-acting terminal repeat (TR) sequence and specifically binds TR DNA. *J Virol* 75:3250–3258.
19. Komatsu T, Ballestas ME, Barbera AJ, Kelley-Clarke B, Kaye KM (2004) KSHV LANA1 binds DNA as an oligomer and residues N-terminal to the oligomerization domain are essential for DNA binding, replication, and episome persistence. *Virology* 319:225–236.
20. Ye FC, et al. (2004) Disruption of Kaposi's sarcoma-associated herpesvirus latent nuclear antigen leads to abortive episome persistence. *J Virol* 78:11121–11129.
21. Juillard F, Tan M, Li S, Kaye KM (2016) Kaposi's sarcoma herpesvirus genome persistence. *Front Microbiol* 7:1149.
22. Gao SJ, et al. (1996) KSHV antibodies among Americans, Italians and Ugandans with and without Kaposi's sarcoma. *Nat Med* 2:925–928.
23. Kedes DH, et al. (1996) The seroepidemiology of human herpesvirus 8 (Kaposi's sarcoma-associated herpesvirus): Distribution of infection in KS risk groups and evidence for sexual transmission. *Nat Med* 2:918–924.
24. Moore PS, et al. (1996) Primary characterization of a herpesvirus agent associated with Kaposi's sarcomae. *J Virol* 70:549–558.
25. Simpson GR, et al. (1996) Prevalence of Kaposi's sarcoma associated herpesvirus infection measured by antibodies to recombinant capsid protein and latent immunofluorescence antigen. *Lancet* 348:1133–1138.
26. Adang LA, Parsons CH, Kedes DH (2006) Asynchronous progression through the lytic cascade and variations in intracellular viral loads revealed by high-throughput single-cell analysis of Kaposi's sarcoma-associated herpesvirus infection. *J Virol* 80:10073–10082.
27. Cotter MA, Robertson ES (1999) The latency-associated nuclear antigen tethers the Kaposi's sarcoma-associated herpesvirus genome to host chromosomes in body cavity-based lymphoma cells. *Virology* 264:254–264.
28. Kelley-Clarke B, Ballestas ME, Komatsu T, Kaye KM (2007) Kaposi's sarcoma herpesvirus C-terminal LANA concentrates at pericentromeric and peri-telomeric regions of a subset of mitotic chromosomes. *Virology* 357:149–157.
29. Günther T, Grundhoff A (2010) The epigenetic landscape of latent Kaposi sarcoma-associated herpesvirus genomes. *PLoS Pathog* 6:e1000935.
30. Sakakibara S, et al. (2004) Accumulation of heterochromatin components on the terminal repeat sequence of Kaposi's sarcoma-associated herpesvirus mediated by the latency-associated nuclear antigen. *J Virol* 78:7299–7310.
31. Stedman W, Deng Z, Lu F, Lieberman PM (2004) ORC, MCM, and histone hyperacetylation at the Kaposi's sarcoma-associated herpesvirus latent replication origin. *J Virol* 78:12566–12575.
32. Sun R, et al. (2017) Epigenetic landscape of Kaposi's sarcoma-associated herpesvirus genome in classic Kaposi's sarcoma tissues. *PLOS Pathog* 13:e1006167.
33. Watanabe A, et al. (2007) A novel KRAB-Zinc finger protein interacts with latency-associated nuclear antigen of kaposi's sarcoma-associated herpesvirus and activates transcription via terminal repeat sequences. *Virus Genes* 34:127–136.
34. Weidner-Glunde M, Mariggiò G, Schulz TF (2017) Kaposi's sarcoma herpesvirus latency-associated nuclear antigen (LANA): Replicating and shielding viral DNA during viral persistence. *J Virol* 91:e01083-16.
35. Boulanger E, et al. (2005) Mono/oligoclonal pattern of Kaposi sarcoma-associated herpesvirus (KSHV/HHV-8) episomes in primary effusion lymphoma cells. *Int J Cancer* 115:511–518.
36. Grundhoff A, Ganem D (2004) Inefficient establishment of KSHV latency suggests an additional role for continued lytic replication in Kaposi sarcoma pathogenesis. *J Clin Invest* 113:124–136.
37. Stürzl M, Gaus D, Dirks WG, Ganem D, Jochmann R (2013) Kaposi's sarcoma-derived cell line SLK is not of endothelial origin, but is a contaminant from a known renal carcinoma cell line. *Int J Cancer* 132:1954–1958.
38. Piolot T, Tramier M, Coppey M, Nicolas JC, Marechal V (2001) Close but distinct regions of human herpesvirus 8 latency-associated nuclear antigen 1 are responsible for nuclear targeting and binding to human mitotic chromosomes. *J Virol* 75:3948–3959.
39. Domsic JF, Chen HS, Lu F, Marmorstein R, Lieberman PM (2013) Molecular basis for oligomeric-DNA binding and episome maintenance by KSHV LANA. *PLoS Pathog* 9:e1003672.
40. Boettiger AN, et al. (2016) Super-resolution imaging reveals distinct chromatin folding for different epigenetic states. *Nature* 529:418–422.
41. McDonnell AV, Jiang T, Keating AE, Berger B (2006) Paircoil2: Improved prediction of coiled coils from sequence. *Bioinformatics* 22:356–358.
42. Toptan T, Fonseca L, Kwun HJ, Chang Y, Moore PS (2013) Complex alternative cytoplasmic protein isoforms of the Kaposi's sarcoma-associated herpesvirus latency-associated nuclear antigen 1 generated through noncanonical translation initiation. *J Virol* 87:2744–2755.
43. Wong LY, Wilson AC (2005) Kaposi's sarcoma-associated herpesvirus latency-associated nuclear antigen induces a strong bend on binding to terminal repeat DNA. *J Virol* 79:13829–13836.
44. Ponnusamy R, et al. (2015) KSHV but not MHV-68 LANA induces a strong bend upon binding to terminal repeat viral DNA. *Nucl Acids Res* 43:10039–10054.
45. Schalch T, Duda S, Sargent DF, Richmond TJ (2005) X-ray structure of a tetranucleosome and its implications for the chromatin fibre. *Nature* 436:138–141.
46. Chiu YF, Sugden AU, Fox K, Hayes M, Sugden B (2017) Kaposi's sarcoma-associated herpesvirus stably clusters its genomes across generations to maintain itself extrachromosomally. *J Cell Biol* 216:2745–2758.
47. Renne R, et al. (1996) Lytic growth of Kaposi's sarcoma-associated herpesvirus (human herpesvirus 8) in culture. *Nat Med* 2:342–346.
48. Menezes J, Leibold W, Klein G, Clements G (1975) Establishment and characterization of an Epstein-Barr virus (EBC)-negative lymphoblastoid B cell line (BJA-B) from an exceptional, EBV-genome-negative African Burkitt's lymphoma. *Biomedicine* 22:276–284.
49. Brulois KF, et al. (2012) Construction and manipulation of a new Kaposi's sarcoma-associated herpesvirus bacterial artificial chromosome clone. *J Virol* 86:9708–9720.
50. Renne R, et al. (2001) Modulation of cellular and viral gene expression by the latency-associated nuclear antigen of Kaposi's sarcoma-associated herpesvirus. *J Virol* 75:458–468.
51. Kellam P, et al. (1999) Characterization of monoclonal antibodies raised against the latent nuclear antigen of human herpesvirus 8. *J Virol* 73:5149–5155.